Article

UAV and Ground Image-Based Phenotyping: A Proof of Concept with Durum Wheat

Adrian Gracia-Romero [1,2], **Shawn C. Kefauver [1,2]**, **Jose A. Fernandez-Gallego [1,2]**,
Omar Vergara-Díaz [1,2], **María Teresa Nieto-Taladriz [3]** and **José L. Araus [1,2,*]**

[1] Integrative Crop Ecophysiology Group, Plant Physiology Section, Faculty of Biology, University of Barcelona, 08028 Barcelona, Spain; adriangraciaromero@hotmail.com (A.G.-R.); sckefauver@ub.edu (S.C.K.); fernandezgallego@gmail.com (J.A.F.-G.); omarvergaradiaz@gmail.com (O.V.-D.)

[2] AGROTECNIO (Center for Research in Agrotechnology), Av. Rovira Roure 191, 25198 Lleida, Spain

[3] Instituto Nacional de Investigación y Tecnología Agraria y Alimentaria (INIA), Ctra. de la Coruña Km. 7.5, 28040 Madrid, Spain; mtnieto@inia.es

* Correspondence: jaraus@ub.edu; Tel.: +34-608-644-144

Abstract: Climate change is one of the primary culprits behind the restraint in the increase of cereal crop yields. In order to address its effects, effort has been focused on understanding the interaction between genotypic performance and the environment. Recent advances in unmanned aerial vehicles (UAV) have enabled the assembly of imaging sensors into precision aerial phenotyping platforms, so that a large number of plots can be screened effectively and rapidly. However, ground evaluations may still be an alternative in terms of cost and resolution. We compared the performance of red–green–blue (RGB), multispectral, and thermal data of individual plots captured from the ground and taken from a UAV, to assess genotypic differences in yield. Our results showed that crop vigor, together with the quantity and duration of green biomass that contributed to grain filling, were critical phenotypic traits for the selection of germplasm that is better adapted to present and future Mediterranean conditions. In this sense, the use of RGB images is presented as a powerful and low-cost approach for assessing crop performance. For example, broad sense heritability for some RGB indices was clearly higher than that of grain yield in the support irrigation (four times), rainfed (by 50%), and late planting (10%). Moreover, there wasn't any significant effect from platform proximity (distance between the sensor and crop canopy) on the vegetation indexes, and both ground and aerial measurements performed similarly in assessing yield.

Keywords: wheat; grain yield; High-Throughput Plant Phenotyping; UAV; RGB; multispectral; canopy temperature

1. Introduction

Projected changes in temperature and precipitation patterns in the coming decades are positioning the Mediterranean Basin as one of the most prominent climate change hotspots [1], where severe impacts on agriculture are expected [2]. Of particular concern for the Iberian Peninsula is an increase in the frequency and severity of droughts associated with a decrease in precipitation and coupled with an increase in evapotranspiration, caused by rising temperatures [3]. Yields of small-grain cereals, such as wheat, will be largely influenced by these scenarios, especially in the rainfed regions that represent nearly 90% of the land under wheat cultivation (MAPAMA https://www.mapama.gob.es/, 2017), and which are already characterized by low and irregular precipitation events during late spring and summer. Hence, improving crop yield under drought and/or high temperature conditions is the

principal goal for breeders. Durum wheat is, by extension, the main cereal cultivated on the southern and eastern shores of the Mediterranean Basin and one of the main cereals in southern Europe [4].

Yield is a phenotypically complicated trait, not only because of its genetic complexity [5], but also due to the relative magnitude of gene–environment interactions [6,7], and it is one of the most integrative traits influenced by known and unknown factors. Thus, genotype evaluations in multi-environment trials are needed, at least in the advanced (generations) stages of selection. However, the major point at issue is that high-throughput plant phenotyping (HTPP) may still represent a bottleneck in breeding programs [7], owing to the need to increase the accuracy, precision, and throughput of the methodologies used, while reducing costs and minimizing labor [8,9]. Furthermore, HTPP approaches should allow multi-temporal trait-specific measurements to evaluate the yield components at different phenological moments.

Nowadays, and almost by definition, HTPP implies the use of non-invasive remote sensing approaches of different nature [5,10], given the possibility of screening larger populations faster than conventional phenotyping procedures. Moreover, recent progress and advances in the technology of aeronautics and sensors have allowed the adoption of unmanned aerial vehicle (UAV) platforms, capable of precisely screening hundreds of plots in a short period of time [7,11]. Further benefits of the simultaneous characterization of many plots are found by minimizing the effect of the changing environmental conditions associated with time-consuming ground measurements. This is evident especially when measuring the canopy temperature [12], which greatly varies throughout the day. In recent years, a considerable bulk of the literature has clearly demonstrated the potential of unmanned airborne platforms for large-scale crop monitoring, mainly due to the high spatial and spectral resolution of the sensors [13,14]. So far, the implementation of aerial platforms in HTPP programs has been extensive and successful in assessing crop performance under different management conditions. As a counterpart, even if potentially of lower throughput, ground-based phenotyping on single plots using cameras or sensors held by hand [15–17] or a pole [18] represent low-cost alternatives to aerial assessments. In addition, shorter distances between sensors and plant targets increase the data spatial resolution [19].

The formulation of different wavelength indexes derived from multispectral and hyperspectral sensors and cameras is well established, and their applications to phenotyping range from measurements of biomass (e.g., normalized difference vegetation index, NDVI [20]) or water content (e.g., water band index, WBI [21]), to assessments of pigment composition (e.g., modified chlorophyll absorption ratio index, MCARI [22]). Canopy temperature measurements are used for the detection of changes in stomatal conductance and transpiration rates, as a response to the water status of the plant [23,24]. At present, the use of red–green–blue (RGB) images may represent a low-cost alternative to the expensive tools just mentioned [25]. The implementation of visible imaging has been extensive and successful for providing a wide range of phenomic data to assess aspects related to the architecture and the color of the plant [26].

All these remote sensing HTPP methodologies are amenable to high-throughput phenotyping in multi-environment trials. Identifying and monitoring plant parameters critical to assessing crop production at key developmental stages will be of great assistance to model and predict yields. The novelty of this study, with respect to recently published work, is that it compares the performance of different UAV remote sensing technologies (RGB, multispectral, and thermal) measured at four different phenological stages for assessing the genotypic performance of durum wheat under a wide range of growing conditions (supplementary irrigation, rainfed, or late-planting). For the processing of this large amount of data we also present the MosaicTool software, for high-throughput data extraction and processing of UAV phenotyping data. The final objective is to provide guidance as to the appropriate RGB, multispectral, and thermal image indexes (i.e., appropriate traits) for the identification of high-yielding as well as resilient varieties. Besides studying phenotypic correlations, the heritability of these traits and their genetic correlations with grain yield have been analyzed. Moreover, the benefits and disadvantages of the use of phenotyping platforms in terms of aerial versus

ground positioning will be evaluated for their potential to discriminate between cultivars and also regarding their throughput capacity and cost.

2. Materials and Methods

2.1. Plant Material, Site Description and Growing Conditions

Twenty-three semi-dwarf varieties of durum wheat (*Triticum turgidum L. subsp durum* (Desf) Husn.) marketed in Spain during the last four decades (Mexa, Vitron, Simeto, Gallareta, Pedroso, Regallo, Arcobaleno, Claudio, Burgos, Dorondon, Avispa, Amilcar, Saragolla, Solea, Euroduro, Don Ricardo, Core, Kiko Nick, Sculpur, Athoris, Don Norman, Olivadur, and Iberus) were evaluated at the experimental station of the Instituto Nacional de Investigación y Tecnología Agraria y Alimentaria (INIA) of Colmenar de Oreja (41°42′44.99″N, 4°41′47.70″O, 590 masl), situated at 40 km south of Madrid (Spain). Climatic data from 2017 was recorded through the Spanish platform SIAR (Servicio de Informacion Agroclimática para el Regadio, www.siar.es) from meteorological stations next to the field. Monthly temperature and rainfall averages are plotted in Figure 1. Colmenar de Oreja presented high temperatures accompanied with low precipitation during the reproductive period (April, May, and the first half of June).
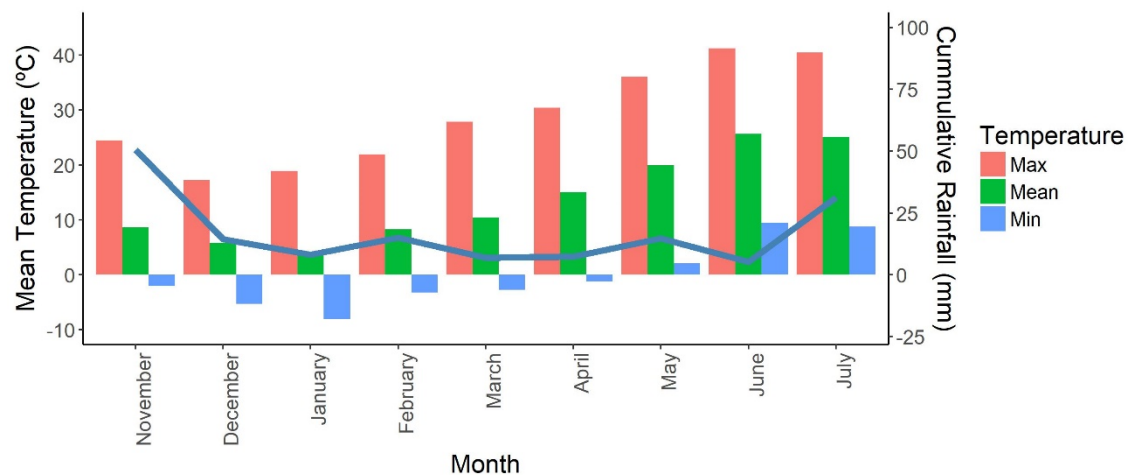

Figure 1. Cumulative monthly rainfall (blue line) and maximum, minimum, and mean temperature (bars) in Colmenar de Oreja for the 2016–2017 crop cycle.

The panel was grown under three different growing treatments: a supplementary irrigation trial, to simulate optimal growing conditions; a rainfed trial without supplementary irrigation, to implement drought stress; and a late-planting trial, leading to higher-than-optimal temperatures throughout the entire crop development period, in order to induce heat stress. The experimental set up consisted of an alpha-lattice design with three replicates in 6 m long and 1.5 m wide plots (a total of 69 plots of 9 m^2), where seeds were planted with a sowing density of 250 seeds m^{-2} in 6 rows per plot on 22 December 2016 for the normal planting trials and on 1 March 2017 for the late-planting. Before sowing, the field was fertilized with 400 kg ha^{-1} of 15:15:15 N:P:K fertilizer (15% N + 15% P$_2$O$_5$ + 15% K$_2$O) and a second application of 150 kg ha^{-1} of urea in a 46% dilution was applied before stem elongation. The rainfed conditions were only provided with one emergency irrigation of 60 mm in order to ensure full plant emergence. Both the supplementary irrigation and late-planting trials were watered every two weeks with irrigations of 60 mm. For all three trials, the crop was harvested on 19 July 2017. Grain yield (GY) (Mg ha^{-1}) was determined for the entire plot, using a harvester. The water content in the grains was between 9.2% and 10.7%.

Aerial and ground phenotyping measurements and sampling were performed during four different visits, planned for assessing crops at the specific development phases of interest (Table 1). At each visit, Zadocks scale values [27] were determined visually for each plot. Moreover, days

after sowing (DAS) and growing degree days (GDD) were counted. GDD was calculated as follows (Equation (1)):

$$GDD = \sum \left(\frac{T_{max} + T_{min}}{2} \right) - T_{base},$$ (1)

where T_{max} corresponds to the highest daily temperature, T_{min} to the lowest, and the T_{base} used was 0 °C.

Table 1. Phenology information of the crop across the measuring/sampling visits, presented as days after sowing (DAS), the growing degree days (GDD), and the developmental period of the crops, expressed with the Zadocks growth scale and the phenological stage.

	Sampling	Date	DAS	GDD	Zadocks Scale	Phen. Stage
Supplementary Irrigation	1st	26/04/2017	125	2224.05	55–59	Heading
	2nd	04/05/2017	133	2399.68	61	Anthesis
	3rd	18/05/2017	147	2767.24	75	Milk Grain Filling
	4th	06/06/2017	166	3377.17	87	Senescence
Rainfed	1st	26/04/2017	125	2224.05	55–57	Heading
	2nd	04/05/2017	133	2399.68	61–65	Anthesis
	3rd	18/05/2017	147	2767.24	77–79	Late Grain Filling
	4th	06/06/2017	166	3377.17	90–99	Senescence
Late-Planting	1st	26/04/2017	56	1270.57	30–32	Stem Elongation
	2nd	04/05/2017	64	1446.21	45–47	Booting
	3rd	18/05/2017	78	1813.76	58–59	Heading
	4th	06/06/2017	97	2423.69	75–79	Milk Grain Filling

2.2. Aerial Platform Description and Orthomosaic Reconstruction Procedure

The aerial UAV system, also commonly known as a drone, was an eight rotor Mikrokopter Oktokopter 6S12 XL (HiSystems GmbH, Moomerland, Germany). Flights were performed under clear sky conditions, with image data captured at an altitude of 50 m. The payload configuration allowed the measurements to be gathered in two flights per trial: the first included the red–green–blue (RGB) cameras, and the second one with both multispectral and thermal cameras that were mounted at the same time. An active two servo gimbal was used to correct for the effect of pitch and roll movements during the flight. Pre-processed aerial images from each sensor were combined to obtain an accurate orthomosaic (Figure 2) by producing a 3D reconstruction with Agisoft PhotoScan Professional software (Agisoft LLC, St. Petersburg, Russia, www.agisoft.com) [28]. To that end, images with at least 80% overlap were used (Table 2). Then, regions of interest corresponding to each plot were segmented and exported using the MosaicTool (Shawn C. Kefauver, https://integrativecropecophysiology.com/software-development/mosaictool/, https://gitlab.com/sckefauver/MosaicTool, University of Barcelona, Barcelona, Spain) integrated as a plugin for the open source image analysis platform FIJI (Fiji is Just ImageJ; http://fiji.sc/Fiji).

Table 2. Number of images comprising each orthomosaic. *, the values refer to the flights conducted over the late-planting trial.

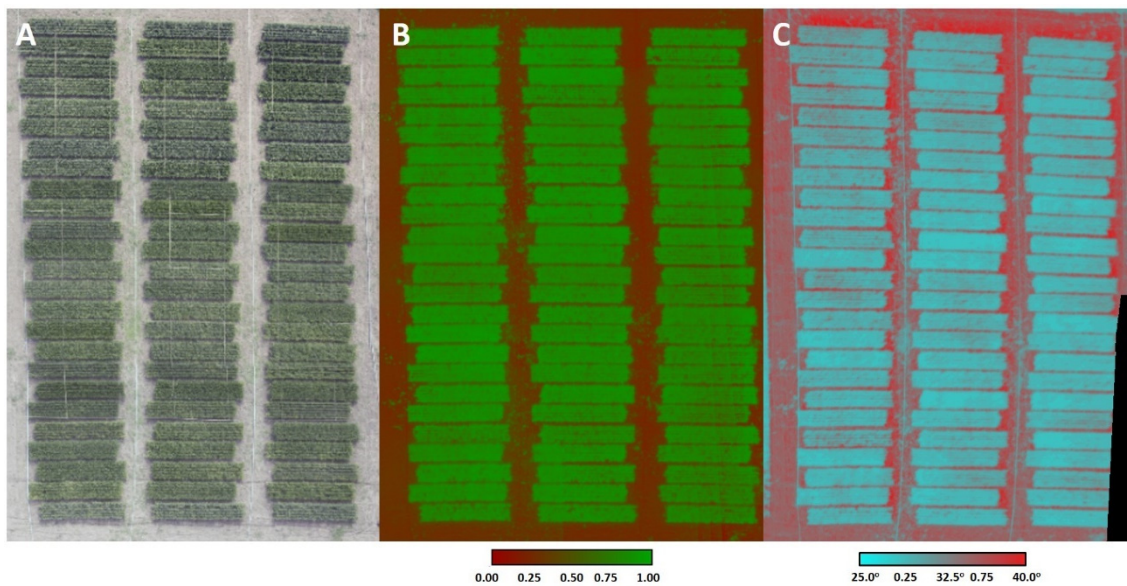| Date of Sampling	RGB	Multispectral	Thermal
26/04/2017	133	24 *	543 *
04/05/2017	184	61	605
18/05/2017	182	71	804
06/06/2017	97 *	36 *	585 *

Figure 2. Red–green–blue (RGB) (**A**), false-color normalized difference vegetation index (NDVI) (**B**), and false-color thermal (**C**) orthomosaic examples corresponding to the late-planting trial during the heading stage at the third sampling visit. Both the multispectral and thermal mosaics have been given false colors: in the former, low NDVI values have been colored red and high values colored green, in the latter, warmer temperature values have been colored red and the colder values colored blue.

2.3. RGB Vegetation Indixes

Vegetation indexes derived from RGB images were evaluated for each plot, from the ground and aerially. At ground level, one picture was taken per plot, holding the camera at 80 cm above the plant canopy, in a zenithal plane and focusing near the center of each plot between 11:00 and 13:00 h. To facilitate the procedure, the camera was attached to a monopod Sony Monopod VCTMP1 (Sony Corporation, Minato, Japan) to adjust and to stabilize the distance between the camera and the top of the canopy to 1 m (Table 3). The conventional digital camera used was a 20.1-megapixel Sony ILCE-QX1 (Sony Corporation, Minato, Japan), with images saved in JPEG format at a resolution of 4608 × 3072 pixels. Aerial RGB images were obtained using a 16-megapixel Lumix GX7 (Panasonic, Osaka, Japan) and saved in JPEG format at a resolution of 4592 × 3448 pixels. According to the used camera, the ground sample distance (GSD) for a flight of 50 m altitude was 0.941 cm/pixel. The color calibration of both cameras with the ColorChecker Passport Photo (X-Rite, Inc., USA) reported correlations R^2 between 0.88 and 0.94 for all the RGB parameters (data not shown).

Segmented ground and aerial images were subsequently analyzed using the MosaicTool plugin. This software includes a JAVA8 version of Breedpix 2.0 (Jaume Casadesús, https://bio-protocol.org/e1488, IRTA, Lleida, Spain) that enables the extraction of RGB indexes in relation to different color properties of potential interest [29]. Derived from the HIS (hue–intensity–saturation) color space, average values from all the pixels of the image were determined for hue, referring to the color tint; saturation, an indication of how much the pure color is diluted with white color; and intensity, as an achromatic measurement of the reflected light. In addition, the portion of pixels with hue classified as green was determined with the green area (GA) and greener area (GGA) indexes. GA is the percentage of pixels in the image with a hue range from 60° to 180°, including yellow to bluish-green color values. Meanwhile, GGA is more restrictive, because it reduces the range from 80° to 180°, thus excluding the yellowish-green tones. Both indexes are also used for the formulation of the crop senescence index (CSI) [30], which provides a scaled ratio between yellow and green pixels to assess the percentage of senescent vegetation. From the CIELab and the CIELuv color space models (recommended by the International Commission on Illumination (CIE) for improved color chromaticity compared to HIS color space), dimension L* represents lightness and is very similar to intensity from the HIS color

space, whereas a* and u* represent the red–green spectrum of chromaticity, and b* and v* represent the yellow–blue color spectrum [31]. Besides the Breedpix indexes mentioned, two other indexes were measured with digital values of the red, green, and blue bands derived from the RGB color model. The normalized green–red difference index (NGRDI) is similar to the NDVI, but uses green instead of near-infrared (NIR) bands [32]. The triangular greenness index (TGI) estimates chlorophyll content based on the area of a triangle with the three points corresponding to the red, green, and blue bands [33].

Table 3. Sensors and cameras used during this experiment and their major specifications.

Measure	Sensor/Camera and Approximated Cost	Image	Major Specifications
RGB indexes	Sony ILCE-QX1 <500 €		20.1 Megapixel. Sensor size: 23.20 × 15.40 mm. Focal length: 35 mm. Trigged and exposure time. programed in automatic mode.
	Panasonic Lumix GX7 <500 €		16 Megapixels. Sensor size: 17.3 × 13.0 mm. Focal length: 35 mm. Trigged and exposure time programed in automatic mode.
Multispect. indexes	Tetracam micro-MCA12 <25,000 €		Incident Light Sensor (ILS). 15.6 Megapixels. Sensor size: 6.66 × 5.32 mm. Wavelengh range: 450 to 950 nm.
	Trimble GreenSeeker Handheld Crop Sensor <500 €		Wavelength range: 670 and 840 nm. Field of view: 25 cm (1 m from the canopy).
Canopy temperature	Raytek PhotoTempTM MXSTM TD infrared thermometer <300 €		Temperature range: −30 to 900 °C. Wavelength range: 8 to 14 μm.
	FLIR Tau2 640 thermal imaging camera < 8000 €		With a VOx uncooled microbolometer equipped with a TeAx Thermal Capture 2.0. Temperature range: −55 to 95 °C. Wavelength range: 7.5 to 13.5 μm.
Pigment content	Dualex Force-A <4000 €		Measured area: 5 mm in diameter Sample thickness: 1 mm maximum Light sources: 5 LED; 1 UV-A, 1 red and 2 near NIR (near-infrared)

2.4. Multispectral Vegetation Indexes

The normalized difference index was determined first at ground level (NDVI.g) for each plot using a portable active sensor, the GreenSeeker handheld crop sensor (Trimble, Sunnyvale, CA, USA), by passing the sensor over the middle of each plot at a constant height of 0.5 m above and perpendicular to

the canopy, between 11:00 to 13:00 h. Alongside this, a Tetracam micro-MCA (Multiple Camera Array) 12 (Tetracam Inc., Chatsworth, CA, USA) was used for assessment of the aerial multispectral data. The camera consists of twelve independent image sensors and optics, each with user configurable filters of center wavelengths and full-width half-max bandwidths (450 ± 40, 550 ± 10, 570 ± 10, 670 ± 10, 700 ± 10, 720 ± 10, 780 ± 10, 840 ± 10, 860 ± 10, 900 ± 20, 950 ± 40 nm). The images captured were passed to twelve separate flash memory cards. Moreover, it has one camera sensor dedicated to ILS (incident light sensor) facing upwards, that uses micro-filters to provide an accurate band-by-band reflectance calibration in real-time. The flights with the multispectral camera were performed at noon (between 12:00 and 14:00 h). After flights for data acquisition, the multispectral images from each band were aligned and calibrated to reflectance using PixelWrench II version 1.2.2.2 (Tetracam, Chatsworth, CA, USA). A suite of multispectral indexes was calculated from the different bands using custom code developed in FIJI and integrated within the MosaicTool software. The formulation of both the RGB and multispectral indexes is detailed in Table 4.

Table 4. Indexes derived from the RGB and multispectral cameras. The wavelengths used in the formulation of the multispectral indexes have been adapted slightly based on the multispectral micro-MCA Tetracam camera. * Note that for the PRI index, B550 is used instead of the original B531 by the cited reference study.

Target Group	Index	Formula	Type; Bands	Ref
Vegetation cover	Green Area (GA)	$60^o < Hue < 180^o$	RGB; HIS color model	[29]
	Greener Area (GGA)	$80^o < Hue < 180^o$	RGB; HIS color model	[29]
Greenness	Crop Senescence Index (CSI)	$\frac{(GA-GGA)}{GA}$	RGB; HIS color model	[30]
	a*; b*		RGB; CIElab color model	[29]
	u*; v*		RGB; CIEluv color model	[29]
	Normalized Green-Red Difference Index (NGRDI)	$\frac{(Green\ DN - Red\ DN)}{(Green\ DN + Red\ DN)}$	RGB; Red and Green bands	[33]
	Triangular Greenness Index (TGI)	$-0.5 \cdot [190 \cdot (Red\ DN - Green\ DN) - 120 \cdot (Red\ DN - Blue\ DN)]$	RGB; Red, Green and Blue bands	[33]
	Normalized Difference Vegetation Index (NDVI)	$\frac{(B840 - B670)}{(B840 + B670)}$	Multispectral; Red, NIR	[34]
	Soil Adjusted Vegetation Index (SAVI)	$\frac{(1+L)\cdot(B840 - B670)}{(B840 + B670\ +\ L)}$ Intermediate vegetation, $L = 0.5$	Multispectral; Red, NIR	[35]
	Optimized soil-adjusted vegetation index (OSAVI)	$\frac{(B780 - B670)}{(B780 + B670 + 0.16)}$	Multispectral; Red, NIR	[36]
	Renormalized Difference Vegetation Index (RDVI)	$\frac{(B840 - B670)}{\sqrt{(B840 + B670)}}$	Multispectral; Red, NIR	[37]
	Enhanced Vegetation Index (EVI)	$\frac{2.5 \cdot (B840 - B670)}{(B840 + (6 \cdot B670) - (7.5 \cdot B45))}$	Multispectral; Blue, Red, NIR	[38]

Table 4. *Cont.*

Target Group	Index	Formula	Type; Bands	Ref
Leaf Pigments	Modified Chlorophyll Absorption Ratio Index (MCARI)	$(B700 - B670) - 0.2 \cdot (B700 - B550) \cdot \left(\frac{B700}{B670}\right)$	Multispectral; Green, Red, NIR	[22]
	Transformed Chlorophyll Absorption Index (TCARI)	$3 \cdot (B700 - B670) - 0.2 \cdot (B700 - B550) \cdot \left(\frac{B700}{B670}\right)$	Multispectral; Green, Red, NIR	[39]
	TCARI/OSAVI ratio	$\frac{TCARI}{OSAVI}$	Multispectral; Green, Red, NIR	[39]
	Anthocyanin Reflectance Index 2 (ARI2)	$B840 \cdot \left(\frac{1}{B550} - \frac{1}{B700}\right)$	Multispectral; Blue, Red, NIR	[40]
	Carotenoid Reflectance Index 2 (CRI2)	$\left(\frac{1}{B550} - \frac{1}{B700}\right)$	Multispectral; Blue, Red	[41]
Photosynthetic Activity	Photochemical Reflectance Index (PRI)*	$\frac{(B550 - B570)}{(B550 + B570)}$	Multispectral; Green	[42]
	Chlorophyll Carotenoid Index (CCI)	$\frac{(B550 - B670)}{(B550 + B670)}$	Multispectral; Green, NIR	[43]
Water content	Water Band Index (WBI)	$\frac{(B970)}{(B900)}$	Multispectral; NIR	[21]

2.5. Canopy Temperature

Canopy temperature (CT) was measured at noon (12:00–14:00 h) from ground level and aerially. For the ground measurements, a PhotoTempTM MXSTM TD infrared thermometer (Raytek, Santa Cruz, USA) was used, pointing towards the canopy at a distance of about 1 m and in the opposite direction to the sun. Simultaneously, air temperature was measured across the plots using a thermos-hygrometer (Testo 177-H1 Logger, Lenzkirch, Germany). The difference between the ambient and the canopy temperature, known as the canopy temperature depression (CTD) [44], was calculated as follows (Equation (2)):

$$CTD = AT - CT. \tag{2}$$

For the aerial measurements, the canopy temperature was measured using a FLIR Tau2 640 thermal imaging camera (FLIR Systems, Nashua, NH, USA) with a VOx uncooled microbolometer equipped with a TeAx Thermal Capture 2.0 (TeAx Technology, Wilnsdorf, Germany), for recording full resolution thermal video (640 × 520 pixels at 20 frames per second). This camera included a thermal couple sensor that measured the actual temperature of the camera sensor, which was used to correct for temperature fluctuations of the VOx sensor during the flight. The thermal images were first exported using TeAx ThermoViewer v1.3.12 software (TeAx Technology, Wilnsdorf, Germany) in raw 16-bit TIFF format as Kelvin × 10,000, and converted to 32-bit temperatures in celsius using a custom batch processing macro function in FIJI [45], also integrated within the MosaicTool software. CT aerial measurements corresponded to average temperature over all the pixels of the plot images. CTD was also calculated using the UAV CT data using the same formula as in Equation (2).

2.6. Leaf Pigment Assessment

Leaf pigment contents were measured using a leaf-clip portable sensor Dualex Force-A (Dualex, Orsay, France) that measured chlorophyll non-destructively, and flavonoids and anthocyanins, as

unitless indexes [46]. In addition, it calculated the nitrogen balance index (NBI), which is the chlorophyll/flavonoids ratio related to the nitrogen and carbon allocation [47]. The Dualex operated with a UV excitation beam at 357 nm, corresponding to the maximum absorption for flavonoids; another LED that operated in the green band for anthocyanins; a red reference beam at 650 nm, corresponding to the absorption for chlorophyll; and two other references in the near-infrared. For each plot, five flag leaves were selected randomly, and the values were averaged. The measurements were done at the adaxial leaf side and in a middle position of the blade between the leaf base and the apex. Dualex measurements were carried out from 10:00 to 12:00 h.

2.7. Statistical Analysis

Data was analyzed statistically using the open source software R [48] and RStudio 1.0.44 [49] (R Foundation for Statistical Computing, Vienna, Austria). Means and standard errors of the GY and all the measurements and indexes were calculated. The effects of growing conditions (water regime and late-planting), genotypes, and their interaction with GY and the remote sensing measurements were determined through a two-factor analysis of variance (ANOVA) for each sample. Differences were considered significant at *p*-value ≤ 0.05. Fisher's LSD (Least significant difference) test was used to determine post hoc differences at each growing condition between the cultivars. To analyze the relationship between the measurements and GY, bivariate Pearson correlation coefficients were calculated. For a further dissection of the genotypic effect on these correlations, broad-sense heritabilities (H^2) and genetic correlations (r_g) were computed using Meta-R (Multi-Environment Trial Analysis with R for Windows), version 6.01 [50]. Genetic variance components were computed across the genotypes for each growing condition as the ratio of the square root of the among genotype variance to the mean value of the corresponding GY or measurement across all genotypes and across the interaction of genotypes and replicates. The broad-sense heritability was calculated as follows (Equation (3)):

$$H^2 = \frac{\sigma_g^2}{\sigma_g^2 + \sigma_{g*Rep}^2 + \frac{\sigma_e^2}{n_{Rep}}}, \tag{3}$$

where σ_g^2, σ_{g*Rep}^2, and σ_e^2 are the genotype, genotype*replicate, and error variance components, and n_{Rep} is the number of replicates. Genetic correlations (r_g) between remote sensing indices and GY were calculated as follows (Equation (4)):

$$r_g = \frac{COV_{Index*GY}}{\sqrt{\sigma_{Index}^2 + \sigma_{GY}^2}}, \tag{4}$$

where $COV_{index*GY}$ is the covariance between the index and the GY, σ_{index}^2 is the variance component of the index, and σ_{gy}^2 is the variance component of GY.

3. Results

3.1. Effects of the Growing Conditions on Yield

Significant differences in grain yield were reported in relation to the growing conditions and the genotypes used (Table 5). The highest-yielding conditions were found under normal planting supported with irrigation—lack of irrigation reduced the yield by almost half. The heat stress effect caused by late-planting also reduced the yields of all the genotypes in comparison to the normal planting with supplementary irrigation conditions.

Table 5. Grain yield (Mg/ha) of the set of modern (semi dwarf) durum wheat cultivars across the imposed growing conditions. Cultivars are ordered from the highest-yielding to the lowest. Values are mean ± standard error of three replicates per cultivar. Different letters (a, b, c, d) indicate significant differences between cultivars within each growing condition according to Fisher's LSD test. Significance levels of the ANOVAs: ** $P < 0.01$; *** $P < 0.001$.

Supplementary Irrigation		Rainfed		Late-Planting	
Olivadur	6.03 ± 0.18 a	Olivadur	3.58 ± 0.13 a	Euroduro	5.06 ± 0.07 a
Burgos	5.67 ± 0.23 ab	Athoris	3.28 ± 0.08 ab	Burgos	4.87 ± 0.12 ab
Sculpur	5.34 ± 0.03 abc	Claudio	3.22 ± 0.10 ab	Claudio	4.62 ± 0.08 abc
Euroduro	5.31 ± 0.12 abc	Kiko Nick	3.14 ± 0.14 ab	Olivadur	4.44 ± 0.09 abcd
Iberus	5.21 ± 0.06 abc	Avispa	3.08 ± 0.17 ab	Sculpur	4.31 ± 0.05 abcd
Claudio	5.19 ± 0.07 abc	Burgos	3.06 ± 0.11 ab	Iberus	4.21 ± 0.13 bcde
Vitron	5.14 ± 0.12 abc	Amilcar	3.06 ± 0.06 ab	Athoris	4.19 ± 0.04 bcde
Athoris	5.08 ± 0.22 abc	Dorondon	3.04 ± 0.07 ab	Solea	4.01 ± 0.12 cdef
Kiko Nick	5.07 ± 0.19 abc	Sculpur	2.88 ± 0.05 abc	D. Norman	3.98 ± 0.03 cdef
Regallo	5.02 ± 0.14 abc	Regallo	2.83 ± 0.15 abc	Regallo	3.89 ± 0.11 cdefg
Dorondon	4.96 ± 0.16 abcd	Vitron	2.81 ± 0.08 abc	Vitron	3.78 ± 0.02 cdefg
Pedroso	4.92 ± 0.22 abcd	Iberus	2.73 ± 0.15 abcd	Saragolla	3.74 ± 0.17 defgh
Amilcar	4.80 ± 0.11 abcd	D. Ricardo	2.72 ± 0.14 abcd	D. Ricardo	3.69 ± 0.11 defghi
Avispa	4.76 ± 0.16 abcd	Euroduro	2.65 ± 0.10 abcd	Dorondon	3.50 ± 0.10 efghi
Saragolla	4.74 ± 0.17 abcd	D. Norman	2.63 ± 0.12 abcd	Kiko Nick	3.45 ± 0.10 efghi
Gallareta	4.71 ± 0.25 abcd	Simeto	2.59 ± 0.20 abcd	Gallareta	3.43 ± 0.11 efghi
Mexa	4.59 ± 0.13 abcd	Gallareta	2.57 ± 0.06 abcd	Avispa	3.24 ± 0.05 fghi
Sole	4.55 ± 0.17 abcd	Mexa	2.52 ± 0.12 abcd	Amilcar	3.18 ± 0.06 ghi
D. Ricardo	4.48 ± 0.06 bcd	Pedroso	2.50 ± 0.11 abcd	Mexa	3.08 ± 0.13 hi
Simeto	4.11 ± 0.14 cd	Arcobaleno	2.34 ± 0.15 bcd	Arcobaleno	3.08 ± 0.05 hi
D. Norman	4.10 ± 0.09 cd	Saragolla	2.27 ± 0.14 bcd	Pedroso	3.06 ± 0.07 hi
Arcobaleno	4.05 ± 0.11 cd	Solea	1.82 ± 0.06 cd	Simeto	2.95 ± 0.08 i
Core	3.46 ± 0.04 d	Core	1.61 ± 0.08 d	Core	3.05 ± 0.18 hi
Mean	4.84 ± 0.04	Mean	2.74 ± 0.04	Mean	3.78 ± 0.04
ANOVA	0.003 **	ANOVA	0.002 **	ANOVA	0.000 ***

3.2. Phenotypic Variability of the Vegetation Indexes, Canopy Temperature, and Pigment Measurements Assessing GY Differences

Over the growing season, large amounts of phenotypic data were generated from each of the experimental conditions (Supplementary Tables S1–S5). The performance of the remote sensing indexes varied considerably across the growing conditions. Differences in the relationships of the indexes with yield underlay the variation in phenology (Figure 3). For most of the indexes calculated there was a genotypic growing effect, particularly for the RGB and multispectral measurements. Genotypic differences in the thermal approximations were clearly found at the beginning of heading in the rainfed trial. For the rest of the conditions, genotypic differences in the CT were only revealed for the aerial measurements.

Under the high-yielding conditions corresponding to the support irrigation plots, all of the measured indexes presented significant correlations to yield before anthesis. GA was the RGB index measured from ground that best correlated with GY during anthesis (r = 0.545), increasing in strength at grain filling (r = 0.684) and decreasing again with maturity (r = 0.435). In terms of multispectral measurements, during anthesis the correlations obtained were very low but increased during grain filling (Figure 4), with the best GY assessments being achieved by the NDVI (r = 0.639 measured from the ground, and r = 0.545 aerially) and its reformulations, the soil adjusted vegetation index (SAVI, r = 0.651) and the renormalized difference vegetation index (RDVI, r = 0.647). The thermal measurements showed a negative correlation with GY but the correlation coefficients were low. Finally, no significant correlations were reported from the pigment measurements derived from the Dualex (Supplementary Table S6).
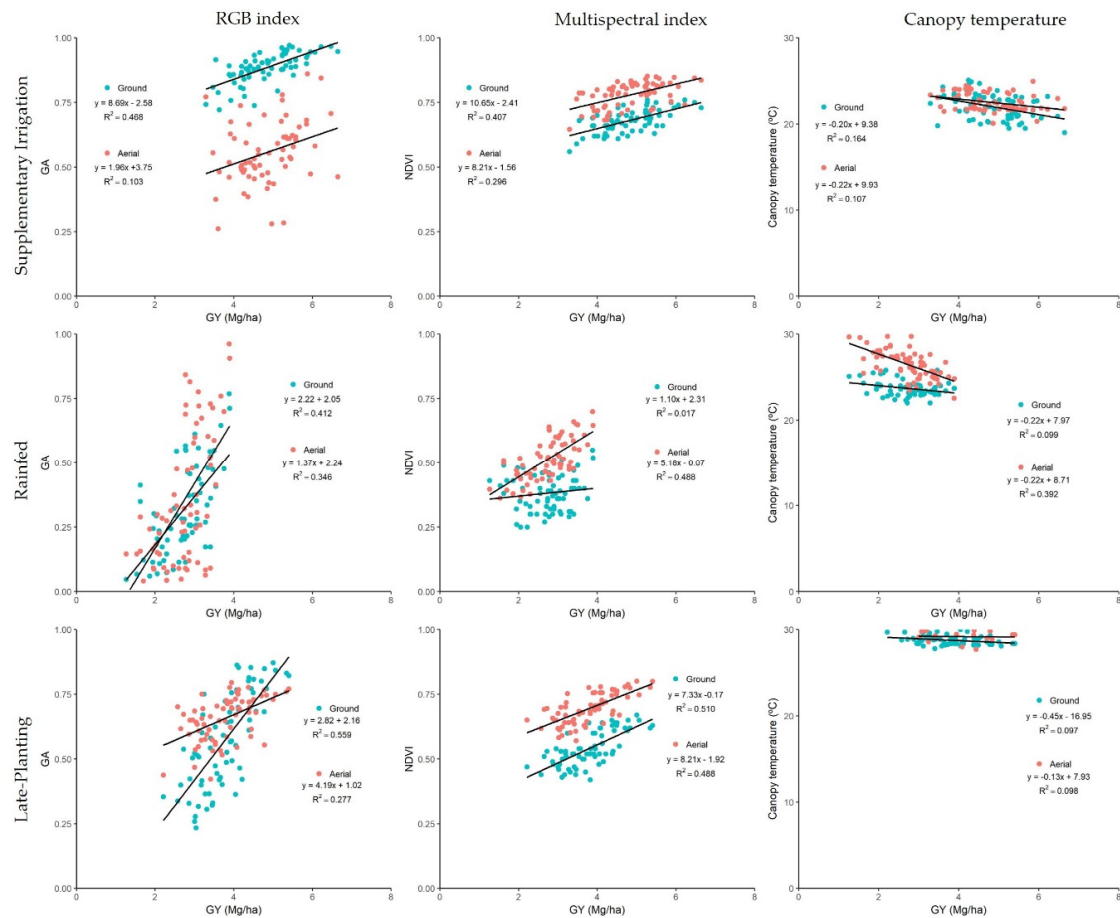
Figure 3. Pearson correlation coefficient heatmap of grain yield with parameters measured from ground and aerial platforms throughout the different phenological stages and treatments. Correlations are scaled according to the key above. Correlations were studied across the 72 plots from each growing condition.

Higher correlations were reported in the rainfed trial than in the supplementary irrigation trial. During heading, the indexes derived from the UAV with the RGB camera were u* (r = −0.609) and NGRDI (r = 0.684). Similar to the supplementary irrigation conditions, the RGB indexes that best correlated with GY during anthesis were GA (r = 0.665) and GGA (r = 0.643), both measured at ground level. Using the aerial images, only GGA remained highly significant (r = 0.565). At grain filling, both ground and aerial RGB indexes had correlations that were very similar to those produced by anthesis data. During maturity, all of the indexes derived from the ground RGB images were closely correlated with GY. As happened within the supplementary irrigation conditions, the NDVI and its reformulations (SAVI, optimized soil-adjusted vegetation index (OSAVI), and RDVI) were the best indexes in assessing GY, showing correlation coefficients higher than 0.630 at anthesis and very close to 0.700 at grain filling. Indexes more targeted towards assessments of the photosynthetic capacity of the crop canopy, such as the photochemical reflectance index (PRI) at grain filling (r = 0.662) and the chlorophyll carotenoid index (CCI) at both anthesis and grain filling (r = 0.548 and r = −0.658, respectively) also correlated with GY. Regarding the thermal measurements, the canopy temperature and aerial measurements of the CTD had high negative correlations with GY at both anthesis (r = −0.762 and r = 0.675, respectively) and at grain filling (r = −0.627 and r = 0.510, respectively). The pigment measurements did not correlate with GY (Supplementary Table S6).

With respect to late-planting, early measurements made during booting showed high correlations with yield using the RGB ground indexes. However, the correlation coefficient values dropped significantly when the indexes were calculated from the aerial HTPP images. Further, during heading, the RGB ground indexes maintained correlation coefficients of similar strength. Finally, the RGB measurements made during the milk grain filling stage, at both ground level and aerially, reported very high correlations with grain yield. The multispectral image indexes followed a very similar pattern to the RGB indexes, with increasing correlation coefficients throughout the crop cycle—from very low correlations at the stem elongation and booting phases to high correlations at heading and at grain filling. The best thermal measurement in terms of assessing GY was reported with CT measurements at heading (r = −0.644). As observed at the other two experimental conditions, the pigment measurements did not correlate with GY (Supplementary Table S6).

Figure 4. Relationships between grain yield with the RGB index green area (GA) (left), the multispectral index NDVI (middle) and the canopy temperature (right), measured from the ground level (red points) and from the aerial level (blue points) during grain filling for the supplementary irrigation (top), the rainfed (middle), and the late-planting (bottom) growing conditions. Correlations were studied across the 72 plots from each growing condition.

3.3. Evaluation of GY and Remote Sensing Traits Heritability

To characterize the impact of the genetic diversity on GY and the remote sensing measurements, broad-sense heritability was estimated. The GY heritability calculated for the stressed conditions corresponding to rainfed conditions ($H^2 = 0.620$) and late-planting ($H^2 = 0.855$) was much higher than the GY heritability calculated for the supplementary irrigation condition ($H^2 = 0.206$). Besides this, to validate the strength of the indexes as predictors of GY differences between genotypes, the products between the broad-sense heritability and the determination coefficient of the genetic correlations ($r_g \times H^2$) were calculated for a selection of measurements that correlated highly to yield (Figure 5). For the support irrigation trial, most of the values of that product exceeded the H^2 of GY, whereas in the case of rainfed conditions, the product values were generally lower than the H^2 of GY, although some were still higher. Regarding late-planting conditions, the indexes during anthesis had lower H^2 and $r_g \times H^2$ products than the H^2 of GY, but both approximations overtook during grain filling.
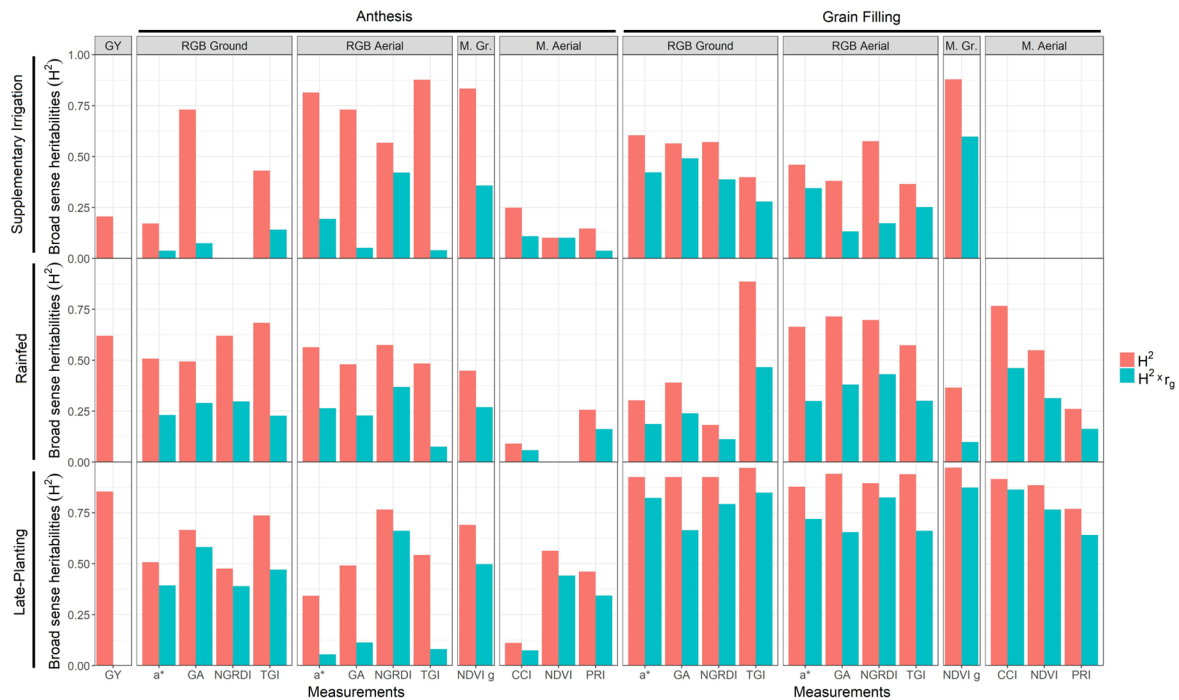
Figure 5. Bar graph comparison of the grain yield and the H^2 (orange) and $H^2 \times r_g$ (blue) indexes of a selection of indexes.

3.4. GY Predictive Models

Using these indexes, which presented the highest correlations with GY at every phenological stage, step-wise linear regression models were calculated in order to generate GY prediction models (Table 6). The results indicated that grain filling was the optimal stage for predicting GY in this study, particularly in the late-planting conditions, where the models explained more than 50% of the yield variability. Additionally, a stepwise analysis was performed within each growing condition, with GY as a dependent variable and the full set of RGB, multispectral, and thermal indexes and measurements from all the sampling dates as independent variables. For the irrigation trial, the equation combined the NGRDI from anthesis, the PRI from grain filling, and the hue from late grain filling. For the rainfed trial, the connection between assessment of the NGRDI at heading, the CT during anthesis, and the NDVI at grain filling far outperformed any of the previous regressions. In the case of late-planting, the combined equation was also a better predictor of GY, using the ground vegetation cover measurement via GGA, the SAVI during anthesis, and the CCI at grain filling.

Finally, for the purpose of testing how accurately the prediction models were, the success rate of prediction for the five highest yielding varieties with each equation was calculated. Most of the equations were correct 60% of the time. Unexpectedly, the equation derived from the CT measurement during anthesis under rainfed conditions, which was the equation explaining most the GY variation, only managed to predict two of the five highest-yielding cultivars correctly. The only equation that achieved a 100% success rate was the one using the CCI during grain filling under late-planting conditions.

Table 6. Multilinear regression (stepwise) of grain yield (GY) as a dependent variable and the remote sensing traits (RGB and multispectral indexes and the thermal measurements) measured both from the ground and aerially as independent variables. Regressions were studied across plots (n = 72) within each growing condition (supplementary irrigation, rainfed, and late-planting). The strength in the prediction of the five highest-yielding cultivars was determined (PS%). R^2, determination coefficient; RSE, residual standard error; A, anthesis; GF, grain filling; LGF, late grain filling; H, heading.

Trial	Phenological Stage	Equation	R^2	RSE	*p*-Value	PS%
Supplementary Irrigation	Anthesis	GY = 64.84 NGRDI + 1.68	0.254	0.652	0.000	60
	Grain Filling	GY = 8.69 GA − 2.85	0.468	0.551	0.000	60
		GY = 0.00096 TGI − 2.00	0.270	0.645	0.000	40
		GY = 12.19 SAVI − 1.83	0.423	0.573	0.000	80
		GY = 26.29 PRI − 0.32	0.287	0.637	0.000	60
	Senescence	GY = 0.07 Hue + 1.98	0.361	0.603	0.000	60
		GY = −0.14 a* + 2.43	0.201	0.675	0.000	60
	Combination	GY = 33.64 NGRDI.A + 11.72 PRI.GF + 0.04 Hue.LGF − 0.92	0.421	0.583	0.000	80
Rainfed	Heading	GY = 0.0009 TGI + 2.00	0.270	0.645	0.000	80
		GY = −0.466 u* − 0.63	0.371	0.478	0.000	40
		GY = 63.80 NGRDI + 0.29	0.468	0.440	0.000	60
	Anthesis	GY = −0.08 u* + 1.83	0.340	0.490	0.000	60
		GY = 4.06 GA − 0.28	0.442	0.450	0.000	60
		GY = 42.97 NGRDI + 1.59	0.453	0.446	0.000	60
		GY = 7.95 NDVI − 3.56	0.440	0.451	0.000	60
		GY = −0.36 CT + 11.71	0.581	0.390	0.000	40
	Grain Filling	GY = −0.10 a* + 2.40	0.413	0.462	0.000	60
		GY = 2.22 GA + 2.02	0.413	0.462	0.000	60
		GY = 7.79 NGRDI + 3.12	0.386	0.472	0.000	60
		GY = 5.18 NDVI + 0.07	0.489	0.431	0.000	60
		GY = 28.12 PRI − 1.67	0.438	0.452	0.000	60
		GY = 8.88 CCI + 1.76	0.433	0.454	0.000	60
		GY = −2.94 TCARIO/SAVI + 4.45	0.488	0.431	0.000	80
	Combination	GY = 22.09 NGRDI.A − 0.28 CT.GF − 0.57 NDVI.GF + 9.45	0.632	0.371	0.000	60
Late-Planting	Heading	GY = −0.11 u* + 1.88	0.366	0.555	0.000	60
		GY = 5.90 GGA − 0.63	0.376	0.551	0.000	60
		GY = 9.19 NGRDI + 1.95	0.349	0.563	0.000	60
	Anthesis	GY = 7.16 GA − 2.38	0.434	0.524	0.000	60
		GY = 64.79 NGRDI + 0.43	0.398	0.541	0.000	80
		GY = 11.52 SAVI − 2.27	0.406	0.537	0.000	80
		GY = −0.43 CT + 15.46	0.414	0.533	0.000	60
	Grain Filling	GY = −0.15 a* + 2.46	0.588	0.447	0.000	80
		GY = 2.82 GA + 2.16	0.559	0.463	0.000	80
		GY = 0.0009 TGI + 1.80	0.533	0.476	0.000	80
		GY = 9.29 SAVI − 0.19	0.563	0.461	0.000	80
		GY = 13.89 CCI + 0.56	0.568	0.458	0.000	100
		GY = −1.08 CRI2 + 6.45	0.488	0.499	0.000	80
	Combination	GY = 1.13 GGA.H + 4.03 SAVI.A + 10.05 CCI.GF − 1.51	0.625	0.433	0.000	80

4. Discussion

4.1. Implications of Growing Conditions on Final GY

Drought (understood as the combination of water stress and heat) and heat stress alone are among the most limiting environmental factors that impact wheat development, inducing many biochemical, molecular, and physiological changes that affect crop yield [51]. In this study, stressed conditions

(rainfed and late-planting) reduced yield substantially in contrast to optimal conditions (supplementary irrigation at the normal planting date), with drought being the most restrictive factor that affected yield. The delay in the sowing date exposed cultivars to increased temperatures during the entire growth cycle, but particularly during the reproductive stages. Meanwhile, grain filling occurred during May in the normal planting trials, with the mean temperature for this month being 19.95 °C; this development stage in the late planting trials took place during late May and the first half of June, and the temperatures rose to 25.62 °C. The temperature established as optimal for the phases of grain filling is around 22 °C and exposure to higher temperatures can significantly decrease GY due to the reduction in the time to capture resources [52]. Moreover, an increase in temperature also results in increases in respiration losses, including dark respiration [53,54] and photorespiration [55], therefore affecting yield negatively. Previous studies have concluded that the response of the crop to shifting the planting date is a region-specific adaptation strongly influenced by climate conditions [56–58]. The loss of yield reported in this study agrees with the model-predicted winter wheat yields in semi-arid regions [59].

4.2. Ability of the Remote Sensing Measurements to Assess Genotypic Differences in Yield under Different Growing Conditions

Given their versatility, remote sensing techniques are currently the most commonly used approaches in HTPP [9], leading to the possibility of generating large amounts of data, as can be observed in this study. The considerable variation in the range of management practices used has greatly influenced wheat cultivar performance, proving that finding the most suitable timing of growth stages to measure remote sensing indexes remains entirely dependent on the target environment [60]. The measurements were performed at critical growth stages for the prediction of yield, as previously reported by Fernandez-Gallego et al. [61]. Post-analysis of this information indicates how crop development can be visualized through the evolution of the indexes and, thus, these trends can be related to crop parameters. Therefore, it is necessary to dissect all these data to determine what needs to be measured, when it needs to be measured, and how it should be measured in relation to our purpose, which in this instance is forecasting yield.

During the phases of ear emergence and flowering, the highest correlations with GY (for the three conditions) were obtained with indexes that were associated with the assessment of vegetation cover. Heading and anthesis are two critical growing stages because an appropriate heading and flowering time will help cultivars maximize their yield potential [62]. As most of the carbohydrates for grain filling are formed after heading [63], a larger leaf area is positively correlated with GY, determining the future number of grains and their weight [64,65]. Derived from the RGB images, the GA and GGA indexes are reliable estimations of the crop coverage of the soil, because they represent the percentage of green pixel values per plot [29,66]. Besides this, vegetation cover can also be determined by assessing how green the plot is on average, such as the a* and u* measurements from the CIElab and the CIEluv color spaces, where the values go from high negative values (green) to low negative or even positive values (lack of green), or the NGRDI index, which is the normalized difference between green and red reflectance. Alongside this, the multispectral indexes use the difference between the NIR and red bands, because this difference is larger for green vegetation and declines to near 0 for soil, making the NDVI suitable for vegetation coverage [67]. The NDVI correlations were improved through the index's reformulations as SAVI and OSAVI, which include parameters for reduction of the brightness effect of the soil [35,36]. In accordance with Duan et al. [68], who dynamically monitored NDVI during a growing season for contrasting wheat cultivars and growing conditions, we also reported a higher correlation with GY during the anthesis period. In most cases, the spectral-resolution precision of the multispectral indexes provides benefits in assessing genotypic differences in GY, but when canopies were found to be very dense (for example under support irrigation during most of the reproductive period), the vegetation indexes reported values near their saturation point. In these cases, the much higher spatial resolution offered by the RBG images allowed indexes like the NGRDI or TGI to perform close to or even surpass the multispectral indexes. However, the values of these

indexes responded greatly to stress applications, with drought and heat stress decreasing the index values notably, exhibiting a wider range of values corresponding to the genotypic performance of the cultivars under each treatment and reporting more robust correlations.

Moving on to grain filling, the total photosynthetically active area (i.e., the green vegetation area) during this stage has been reported as being very closely related to the final GY [69]. The decrease in canopy greenness due to the ripening process was markedly synchronized with the values of the vegetation indexes. Therefore, as senescence varies considerably depending on genotype [70], stay-green and early senescence phenotypes can be easily identified, for example, with the NDVI [71,72]. This is of importance for selecting genotypes with an extended duration of active photosynthesis, particularly under conditions that tend to accelerate senescence [73]. With regard to the assessment of genotypic differences in GY, our results showed that the most suitable phenological stage for conducting measurements was around the last stages of grain filling, detecting genotypic differences in canopy greenness and, thus, stay-green, similar to previous studies monitoring wheat trials repeatedly over the entire growing season [74]. Stay-green has been principally associated with extended periods of photosynthetic activity and maintaining the supply of assimilated carbon in order to ensure that grain mass is maximized. Thus, a longer duration of flag leaf greenness through GF has been associated with an increased yield wheat [75]. Moreover, Christopher et al. [72] also concluded that, for wheat, the high correlations between NDVI and yield obtained during GF were due to the fact that this was the key phenological stage for assessing genotypic differences in senescence dynamics. However, some studies in bread wheat, such as Kichey et al. [76] and Derkx et al. [77] have reported a lack of yield increase while retaining green leaf area for longer during GF. To overcome these inconsistencies may require examining plant biomass, additional information about pigment content, and the regulatory processes of photosynthesis, which could help to further understand the genetic differences in yield.

Indeed, assessing differences in the photosynthetic capacity, independently of the green biomass, can be of a great importance. For instance, changes in photosynthesis nearly parallel changes in chlorophyll content. The chlorophyll-related indices measured (chlorophyll from the leaf sensor, and the TGI, transformed chlorophyll absorption index (TCARI), MCARI, and CCI assessed at the canopy level) showed how the pigment content increased until anthesis, and then started decreasing during grain filling. Regarding its performance in assessing yield, on one side, the leaf relative chlorophyll content measured with the leaf sensor did not correlate well with GY. These readings provide useful information for diagnosing plant N status and, by the time N is a limiting factor, it may work efficiently as a GY predictor [78]. However, without nutrient restrictions, the leaf chlorophyll content–GY relationship is not so clear. Moreover, it is only measured in the flag leaf, not across the canopy. Based on similar results, Monostori et al. [79] concluded that relative chlorophyll content values should be calibrated according to the cultivars used and depending on their performance. On the other hand, chlorophyll measurements derived from the RGB and multispectral images did show some significant correlations with GY. Taking into account that, while pigment-meters like the Dualex estimate the chlorophyll concentration using the last developed leaves and thus the last to senesce, the HTPP reflectance indexes related to pigment content are assessed at the canopy level. Thus, while still being sensitive to chlorophyll content, any differences present in green biomass may also influence the pigment measurements and the indexes will measure the total physical volume of chlorophyll at the canopy.

Apart from chlorophyll assessments, the actual photosynthetic capacity can be determined with the CCI and PRI indexes. Both indexes use narrowband reflectance at 531 nm, located between two broad bands of strong pigment absorption related to chlorophylls a and b, and they help to separate more steady-state photosynthetic pigments from those related to photosynthetic stress and efficiency. The photochemical reflection index (PRI) was formulated to assess how efficiently radiation is used by plants during photosynthesis [80], as it is highly sensitive to changes in the short-term xanthophyll cycle [81]. Distinct from the PRI, the chlorophyll carotenoid index (CCI) also includes information from red reflectance, indicating changes in the chlorophyll to carotenoid ratio [43]. Therefore, these

indexes are suitable measurements for estimation of the photosynthetic variability induced by heat and drought. The best performance of these indexes occurred with measurements made during the grain filling stage, owing to their potential to detect the photoprotective response to excess light [82]. Because radiation is available in excess in the Mediterranean Basin [83], photo-protection mechanisms are needed to prevent cell damage and to ensure that plant metabolism continues normally [42], so radiation use efficiency is a key trait under such conditions [84].

Stomatal regulation is a key determinant of plant photosynthesis and is highly influenced by the surrounding environment. As an alternative to the direct assessment of leaf stomatal conductance, measuring the canopy temperature (CT) provides an instantaneous proxy of plant water status [85]. Stomatal closure induced by environmental stress will cause an increase in leaf temperature. Thus, negative correlations were reported between the canopy temperature and GY. Assuming that the normal season planting and the support-irrigated trial represented close to optimal growing conditions, there should have been no disturbances affecting stomatal conductance. Still, considering the low correlations observed, the pattern observed can be related to the capability of genotypes to be more or less photosynthetically active. Under non-water-limited conditions, a cooler CT has been associated with genetic gains in wheat yield due to higher stomatal conductance and greater maximum photosynthetic rates [86]. On the other hand, the CT correlation with grain yield for the stressed conditions (rainfed and late-planting) was clearly stronger than in the supplemental irrigation trial, which reported negative correlations. The genotypes that produced the lowest GY presented elevated CT during the anthesis and grain filling periods, and vice versa. Hence, genotypes with a higher resistance to drought and heat can be identified as plants with cooler leaves [87]. Therefore, CT measurements characterize the crop physiologically and in a way that is complimentary to assessing plant density or greenness.

To effectively utilize the remote sensing measurements to assess GY, predictive models were calculated using step-wise regressions. Most of the best grain yield predictors obtained were formulated using traits measured during grain filling. Even so, models combining various measurements taken at different phenological stages greatly improved the prediction capacity. The potential yield of a crop is given by the interception of irradiance of the canopy, but it is also determined by the conversion of that irradiance into chemical energy [88]. The incorporation of high-throughput monitoring into prediction models enables more accurate selection of superior breeding lines [89,90]. The models developed here incorporated a vegetation cover measurement during the pre-anthesis and anthesis phases to assess crop density, an approximation of the rate of photosynthesis applied to the estimation of the light use efficiency (PRI, CCI) or the stomatal conductance (CT) during grain filling, and finally a measurement of the delay in senescence of the plants. In accordance with our findings, Crain et al. [74] concluded that NDVI and CT could be used for indirect selection for GY under heat and drought, based on their results of trait heritability and correlation to GY.

4.3. Comparative Performance of Ground Versus Aerially Assessed Indexes

The main benefit of incorporating imaging methodologies into aerial-based platforms is that researchers are then able to cover larger experimental areas in less time, thus minimizing the effects of diurnal variation in environmental variables, like changes in radiation and temperature, or the occurrence of clouds [44]. The aerial indexes worked very similarly to the ground measurements, reinforcing their usefulness for high-throughput plant phenotyping in the field.

As counterbalance to the high-throughput capacity of aerial imaging, the platform distance from the canopy led to a loss in image resolution. In the case of RGB measurements, even though the sensor size of the cameras used was very similar (23.20×15.40 mm for the Sony QX1 and 17.3×13 mm for the Olympus OM-D), the distance between the crop and the camera reduced the resolution of the resulting plot level images when they were captured from the aerial HTPP. As an illustration, while the aerial plot images had a resolution of 473×129 pixels, the resolution of the images taken from the ground was 5456×3632 pixels. Despite this restriction, aerial indexes were still highly correlated with

grain yield, especially at grain filling. The reduction in the number of pixels had a greater effect on the assessments related to fractional vegetation cover, such as the indexes derived from the HIS color model, including information of both vegetation and bare soil [91], so the yield prediction capacities of the GA, GGA, and CSI were generally lower when measured from the aerial platform. The other RGB indexes seemed to be less sensitive to this loss in spatial resolution and were better at maintaining the correlation coefficients across platforms. Besides this, it is also important to take into consideration the fact that aerial images are able to assess the whole plot (therefore overcoming canopy heterogeneity), while the ground-based approaches only allow for assessment of less than a tenth of the total plot, and for this reason more than one measurement may be needed. A similar trend was observed with the NDVI assessments, with the GreenSeeker measurements on the ground being slightly better correlated than the aerial measures derived from the multispectral images. This is because this hand-held sensor produces data covering almost the whole plot, with the final value corresponding to the average of 10–20 measurements captured while walking across the plot. When comparing the performance of CT measured from the ground and aerially for GY, a clear difference was found between the two approaches, with CT measured from the UAV showing better results. Traditionally, hand-held infrared thermometers have been used but they can be problematic in large field studies due to the temporal changes during the time required to measure all plots [12]. Because temperature can fluctuate quickly, it is of profound importance to screen the whole trial as quickly as possible, in order to have comparable data across all the plots. The use of UAVs permits the acquisition of thermal images of a large number of plots in a short time, overcoming this environmental variability restriction.

In that sense, aerial remote sensing platforms are an effective way to rapidly monitor crops, particularly in large fields. However, even when UAVs have reached comparatively affordable prices, the associated cost entailed in their employment still makes them a relatively expensive approach in some cases. Besides the price of the platform and the sensors, it is compulsory to pay for vehicle insurance, and a certified pilot and trained operator must be engaged to carry out the flights. Thus, the implementation of an aerial platform in a phenotyping study might demand a considerable initial investment, but later savings in manpower will compensate for the initial investment because there will be fewer employees to pay. Another aspect to consider is the sizeable technical capacity necessary for data processing, from radiometric calibration of the images and the creation of a georeferenced ortho-mosaic to ensure effective and efficient data extraction and analysis. For these reasons, ground-based or hand-held methodologies might be more feasible alternatives in certain circumstances due to their low cost and ease of management. In addition, most ground-based sensors generate measurements with no need for extra time for data processing and index calculation. As proposed by Araus and Kefauver [9] and applied in this study, an innovative option could be the attachment of a camera to a "pheno-pole". The camera is controlled remotely with a smartphone by Wi-Fi, so it is possible for the pole to be as high as 4 m, allowing measurements of tall crops, like maize or fruit trees. Using ground-based phenotyping methodologies requires more time for data acquisition, but the staff require fewer technical skills, and as indicated above, the post-image treatment is minimal and frequently the software needed for extracting vegetation indices from the images is open access. The RGB indices are clear examples where a range of open access software is already available (https://integrativecropecophysiology.com/software-development/). One last point is that drones as objects in airspace are still under discussion within regulatory frameworks and UAV-related laws are in a constant evolutionary progress [92], thus their full implementation in many countries is limited. For these reasons, users need to take stock of the strengths, opportunities, and limitations associated with each sensor and platform and make a choice depending on their objectives. Future improvements will make these technologies more user-friendly and available for all types of end-users [93], and smartphones may play a central role in these solutions.

The time spent on fieldwork in the current study using the aerial platform for RGB imaging was approximately 10 min, including five minutes for pre-flight preparation procedures and five minutes for the flight itself. Before conducting any flight, it is essential to complete certain pre-flight checklist

tasks to ensure that the flight will perform correctly without any technical incidents. The alignment of the raw images onto georeferenced orthomosaics took 15 min. Finally, the semi-automatic extraction and processing of the data took another 15 min. In contrast, the time required for capturing images manually from the ground or using a hand-held sensor, such as the GreenSeeker or a thermal gun, was around 12 min, and the RGB data processing only took five minutes. Nonetheless, leaf clamp meters like the Dualex require longer periods of time because the estimated time per plot is around one minute to capture at least six individual measurements. In small field trials, the throughput differences between the two approaches might seem small, but in large studies the time/cost differences become much greater. Considering this task's calculated time for aerial images acquisition as a reference, we have simulated how long it would take to measure a larger field of 300 plots. Without changing the plot dimensions, a 300-plot field would cover more or less an area of 0.4 Ha. However, the time would not increase much and in less than 10 min the whole field would be screened. Similarly, the pre-processing would also be increased only a bit.

4.4. Repeatability and Applicability of Remote Sensing Measurements for Assessing GY

Success in collecting accurate phenotyping data is intimately connected with heritability of the trait [94]. Broad-sense heritability is a reflection of both the genetic variance and the level of precision that can be achieved within and across trials [95], and sometimes it is termed as repeatability. The heritability metrics assess the quality of the measurements, and these are a key element for implementing such new technologies in breeding programs, because they will help plant breeders to forecast the grain yield behavior of the succeeding generation. The possibility of being able to promptly evaluate the improvement target, in this case grain yield, with an index would permit breeders to make well-informed decisions about the cultivars. According to the results obtained, the most robust measurements were made in the rainfed and the late-planting trial, during grain filling, increasing the confidence of using such measurements for selection under suboptimal growing conditions. Traditional and time-consuming manual measurements of plant height have been used as selection traits for yield improvement. The high estimates of H^2 reported in our results suggest the possibility of using remote sensing measurements to forecast the grain yield behavior of the succeeding generation.

5. Conclusions

It is particularly important to evaluate the response of the remote sensing indexes to the crop genotypic performance in order to implement correctly those methodologies in phenotyping. Knowing which are the remote sensing parameters that best predict genotypic variability in yield and when to measure them will help to develop accurate yield prediction models for phenotyping, which may help to accelerate the selection process in breeding programs. Moreover, a better understanding of the strengths and limitations of these indices may help to forecast production or to improve crop monitoring associated with management practices. In our study, the performance of the set of vegetation indexes studied varied widely across the growing conditions and the phenological stages. Measurements related to the greenness of the canopy were the best for assessing genotypic differences in GY according to the phenotypic and genotypic correlations and heritabilities calculated, regardless of the nature of the data collected (RGB or multispectral). Furthermore, our results proved that grain filling was the best phenological stage to forecast GY among those evaluated. At the beginning of grain filling, vegetation indexes can assess the amount of biomass present, and thus the photosynthetically active area that contributes to the filling of the grain. Moreover, at the end of the stage, we can evaluate the length of this period and see which cultivars stay green (i.e., photosynthetically active) for longer, with their concomitant delay in senescence. Therefore, the RGB-derived vegetation indexes are presented as the most suitable traits to be measured, because despite being a low-cost tool, this set of indexes performed as well as, and sometimes better than, indexes derived from more expensive devices (i.e., multispectral and thermal indexes). Besides this, when studying crop and genotype responses to drought and heat,

canopy temperature assessed from an aerial platform has proven to be a useful addition to the other two categories of remote sensing techniques.

As has been proven in this work, the ground and aerial measurements performed very similarly in terms of assessing GY. For this reason, when scaling to large scale studies, the selection of the platform may depend not only on its cost, but also the time and skill required to conduct the measurements properly. The only exception is canopy temperature, where the simultaneous evaluation of all the plots from the UAV (T.a) performed much better than the temperature measured sequentially from the ground (T.g) in individual plots.

Supplementary Materials: The following are available online at http://www.mdpi.com/2072-4292/11/10/1244/s1, Table S1: Effect of growing conditions across phenological stages for the RGB indexes assessed from the ground level, Table S2: Effect of growing conditions across phenological stages for the RGB indexes assessed aerially, Table S3: Effect of growing conditions across phenological stages for the multispectral indexes assessed aerially, Table S4: Effect of the growing conditions across phenological stages for the thermal measurements, Table S5: Effect of growing conditions across phenological stages for the Dualex measurements, Table S6: Correlation coefficients of the relationships between the pigment measurements with the Dualex and the GY.

Abbreviations

MAPAMA	Ministerio de Agricultura y Pesca Alimentación y Medio Ambiente
UAV	Unmanned Aerial Vehicle
RGB	Red-Green-Blue
NDVI	Normalized Difference Vegetation Index
GA	Green Area
CCI	Chlorophyll Content Index
TGI	Triangular Greenness Index
GY	Grain Yield
HTPP	High-Throughput Plant Phenotyping
MET	Multi-Environment Trials
INIA	Instituto Nacional de Investigación y Tecnología Agraria y Alimentaria
SIAR	Servicio de Informacion Agroclimática para el Regadio
NBI	Nitrogen Balance Index
CT	Canopy Temperature
CTD	Canopy Temperature Depression
ANOVA	Analysis of Variance
H^2	Heritability

r_g	Genetic Correlations
σ^2_g	Genotype Variance
σ^2_g	Genotype Variance
σ^2_e	Error variance
n	Number of Replicates

References

1. Diffenbaugh, N.S.; Giorgi, F. Climate change hotspots in the CMIP5 global climate model ensemble. *Clim. Chang.* **2012**, *114*, 813–822. [CrossRef]

2. Asseng, S.; Ewert, F.; Martre, P.; Rötter, R.P.; Lobell, D.B.; Cammarano, D.; Kimball, B.A.; Ottman, M.J.; Wall, G.W.; White, J.W.; et al. Rising temperatures reduce global wheat production. *Nat. Clim. Chang.* **2015**, *5*, 143–147. [CrossRef]

3. Vicente-Serrano, S.M.; Lopez-Moreno, J.I.; Beguería, S.; Lorenzo-Lacruz, J.; Sanchez-Lorenzo, A.; García-Ruiz, J.M.; Azorin-Molina, C.; Morán-Tejeda, E.; Revuelto, J.; Trigo, R.; et al. Evidence of increasing drought severity caused by temperature rise in southern Europe. *Environ. Res. Lett.* **2014**, *9*, 1–9. [CrossRef]

4. Royo, C.; Soriano, J.M.; Alvaro, F. Wheat: A Crop in the Bottom of the Mediterranean Diet Pyramid. In *Mediterranean Identities—Environment, Society, Culture*; IntechOpen: London, UK, 2017. [CrossRef]

5. Reynolds, M.; Langridge, P. Physiological breeding. *Curr. Opin. Plant Biol.* **2016**, *31*, 162–171. [CrossRef] [PubMed]

6. Quintero, A.; Molero, G.; Reynolds, M.P.; Calderini, D.F. Trade-o ff between grain weight and grain number in wheat depends on GxE interaction: A case study of an elite CIMMYT panel (CIMCOG). *Eur. J. Agron.* **2018**, *92*, 17–29. [CrossRef]

7. Araus, J.L.; Cairns, J.E. Field high-throughput phenotyping: The new crop breeding frontier. *Trends Plant Sci.* **2014**, *19*, 52–61. [CrossRef] [PubMed]

8. Cobb, J.N.; DeClerck, G.; Greenberg, A.; Clark, R.; McCouch, S. Next-generation phenotyping: Requirements and strategies for enhancing our understanding of genotype-phenotype relationships and its relevance to crop improvement. *Theor. Appl. Genet.* **2013**, *126*, 867–887. [CrossRef]

9. Araus, L.; Kefauver, S.C. Breeding to adapt agriculture to climate change: Affordable phenotyping solutions. *Curr. Opin. Plant. Biol.* **2018**, *45*, 237–247. [CrossRef] [PubMed]

10. Atzberger, C. Advances in Remote Sensing of Agriculture: Context Description, Existing Operational Monitoring Systems and Major Information Needs. *Remote Sens.* **2013**, *5*, 949–981. [CrossRef]

11. Araus, J.L.; Kefauver, S.C.; Zaman-allah, M.; Olsen, M.S.; Cairns, J.E. Translating High-Throughput Phenotyping into Genetic Gain. *Trends Plant Sci.* **2018**, *23*, 451–466. [CrossRef]

12. Deery, D.M.; Rebetzke, G.J.; Jimenez-Berni, J.A.; James, R.A.; Condon, A.G.; Bovill, W.D.; Hutchinson, P.; Scarrow, J.; Davy, R.; Furbank, R.T. Methodology for High-Throughput Field Phenotyping of Canopy Temperature Using Airborne Thermography. *Front. Plant Sci.* **2016**, *7*, 1808. [CrossRef]

13. Yang, G.; Liu, J.; Zhao, C.; Li, Z.; Huang, Y. Unmanned Aerial Vehicle Remote Sensing for Field-Based Crop Phenotyping: Current Status and Perspectives. *Front. Plant Sci.* **2017**, *8*, 1111. [CrossRef]

14. Berni, J.A.J.; Member, S.; Zarco-tejada, P.J.; Suárez, L.; Fereres, E. Thermal and Narrowband Multispectral Remote Sensing for Vegetation Monitoring From an Unmanned Aerial Vehicle. *IEEE Trans. Geosci. Remote Sens.* **2009**, *47*, 1–17. [CrossRef]

15. Yousfi, S.; Kellas, N.; Saidi, L.; Benlakehal, Z.; Chaou, L.; Siad, D.; Herda, F.; Karrou, M.; Vergara, O.; Gracia, A.; et al. Comparative performance of remote sensing methods in assessing wheat performance under Mediterranean conditions. *Agric. Water Manag.* **2016**, *164*, 137–147. [CrossRef]

16. Vergara-Díaz, O.; Zaman-allah, M.A.; Masuka, B.; Hornero, A.; Zarco-Tejada, P.; Prasanna, B.M.; Cairns, J.E.; Araus, J.L. A Novel Remote Sensing Approach for Prediction of Maize Yield Under Different Conditions of Nitrogen Fertilization. *Front. Plant Sci.* **2016**, *7*, 1–13. [CrossRef] [PubMed]

17. Vergara-Díaz, O.; Kefauver, S.C.; Elazab, A.; Nieto-Taladriz, M.T.; Araus, J.L. Grain yield losses in yellow-rusted durum wheat estimated using digital and conventional parameters under field conditions. *Crop J.* **2015**, *3*, 200–210. [CrossRef]

18. Fernandez-Gallego, J.A.; Kefauver, S.C.; Gutiérrez, N.A.; Nieto-Taladriz, M.T.; Araus, J.L. Wheat ear counting in-field conditions: High throughput and low-cost approach using RGB images. *Plant Methods* **2018**, *14*, 22. [CrossRef] [PubMed]

19. Condorelli, G.E.; Maccaferri, M.; Newcomb, M.; Andrade-Sanchez, P.; White, J.W.; French, A.N.; Sciara, G.; Ward, R.; Tuberosa, R. Comparative Aerial and Ground Based High Throughput Phenotyping for the Genetic Dissection of NDVI as a Proxy for Drought Adaptive Traits in Durum Wheat. *Front. Plant Sci.* **2018**, *9*, 1–17. [CrossRef]

20. Tucker, C.J. Red and photographic infrared linear combinations for monitoring vegetation. *Remote Sens. Environ.* **1979**, *8*, 127–150. [CrossRef]

21. Peñuelas, J.; Filella, I.; Biel, C.; Serrano, L.; Savé, R. The reflectance at the 950–970 nm region as an indicator of plant water status. *Int. J. Remote Sens.* **1993**, *14*, 1887–1905. [CrossRef]

22. Daughtry, C.; Walthall, C.L.; Kim, M.S.; Brown de Colstoun, E.; McMurtrey, J.E. Estimating Corn Leaf Chlorophyll Concentration from Leaf and Canopy Reflectance. *Remote Sens. Environ.* **2000**, *74*, 229–239. [CrossRef]

23. Jackson, R.D.; Reginato, R.J.; Idso, S.B. Wheat canopy temperature: A practical tool for evaluating water requirements. *Water Resour. Res.* **1988**, *13*, 651–656. [CrossRef]

24. Moran, M.S.; Clarke, T.R.; Inoue, Y.; Vidal, A. Estimating crop water deficit using the relation between surface-air temperature and spectral vegetation index. *Remote Sens. Environ.* **1994**, *49*, 246–263. [CrossRef]

25. Casadesús, J.; Villegas, D. Conventional Digital Cameras as a Tool for Assessing LAI and Biomass for Cereal Breeding. *New Technol.* **2013**, *56*, 1–27.

26. Gracia-Romero, A.; Kefauver, S.C.; Vergara-Díaz, O.; Zaman-Allah, M.A.; Prasanna, B.M.; Cairns, J.E.; Araus, J.L. Comparative Performance of Ground vs. Aerially Assessed RGB and Multispectral Indices for Early-Growth Evaluation of Maize Performance under Phosphorus Fertilization. *Front. Plant Sci.* **2017**, *8*, 2004. [CrossRef]

27. Zadoks, J.C.; Chang, T.T.; Konzak, C.F. A decimal code for the growth stages of cereals. *Weed Res.* **1974**, *14*, 415–421. [CrossRef]

28. Bendig, J.; Bolten, A.; Bennertz, S.; Broscheit, J.; Eichfuss, S.; Bareth, G. Estimating biomass of barley using crop surface models (CSMs) derived from UAV-based RGB imaging. *Remote Sens.* **2014**, *6*, 10395–10412. [CrossRef]

29. Casadesus, J.; Kaya, Y.; Bort, J.; Nachit, M.M.; Araus, J.L.; Amor, S.; Ferrazzano, G.; Maalouf, F. Using vegetation indices derived from conventional digital cameras as selection criteria for wheat breeding in water-limited environments. *Ann. Appl. Biol.* **2007**, *150*, 227–236. [CrossRef]

30. Zaman-Allah, M.; Vergara, O.; Araus, J.L.; Tarekegne, A.; Magorokosho, C.; Zarco-Tejada, P.J.; Hornero, A.; Albà, A.H.; Das, B.; Craufurd, P.; et al. Unmanned aerial platform-based multi-spectral imaging for field phenotyping of maize. *Plant Methods* **2015**, *11*, 35. [CrossRef] [PubMed]

31. Pointer, M.R. A comparison of the CIE 1976 colour spaces. *Color Res. Appl.* **1981**, *6*, 108–118. [CrossRef]

32. Hunt, R.; Cavigelli, M.; Daughtry, C.; McMurtrey, J.E.; Walthall, C.L. Evaluation of Digital Photography from Model Aircraft for Remote Sensing of Crop Biomass and Nitrogen Status. *Precis. Agric.* **2005**, *6*, 359–378. [CrossRef]

33. Hunt, E.R.; Doraiswamy, P.C.; Mcmurtrey, J.E.; Daughtry, C.S.T.; Perry, E.M.; Akhmedov, B. A visible band index for remote sensing leaf chlorophyll content at the canopy scale. *Int. J. Appl. Earth Obser. Geoinf.* **2013**, *21*, 103–112. [CrossRef]

34. Rouse, J.W.; Hass, R.H.; Schell, J.A.; Deering, D.W. Monitoring vegetation systems in the great plains with ERTS. In Proceedings of the Third Earth Resources Technology Satellite (ERTS) Symposium, Washington, DC, USA, 10–14 December 1973; Volume 1, pp. 309–317.

35. Huete, A. A soil-adjusted vegetation index (SAVI). *Remote Sens. Environ.* **1988**, *25*, 295–309. [CrossRef]

36. Rondeaux, G.; Steven, M.; Baret, F. Optimization of soil-adjusted vegetation indices. *Remote Sens. Environ.* **1996**, *55*, 95–107. [CrossRef]

37. Roujean, J.-L.; Breon, F.-M. Estimating PAR absorbed by vegetation from bidirectional reflectance measurements. *Remote Sens. Environ.* **1995**, *51*, 375–384. [CrossRef]

38. Huete, A.; Didan, K.; Miura, T.; Rodriguez, E.P.; Gao, X.; Ferreira, L.G. Overview of the radiometric and biophysical performance of the MODIS vegetation indices. *Remote Sens. Environ.* **2002**, *83*, 195–213. [CrossRef]

39. Haboudane, D.; Miller, J.R.; Tremblay, N.; Zarco-Tejada, P.J.; Dextraze, L. Integrated narrow-band vegetation indices for prediction of crop chlorophyll content for application to precision agriculture. *Remote Sens. Environ.* **2002**, *81*, 416–426. [CrossRef]

40. Gitelson, A.A.; Merzlyak, M.N.; Chivkunova, O.B. Optical Properties and Nondestructive Estimation of Anthocyanin Content in Plant Leaves. *Photochem. Photobiol.* **2001**, *74*, 38–45. [CrossRef]

41. Gitelson, A.A.; Zur, Y.; Chivkunova, O.B.; Merzlyak, M.N. Assessing carotenoid content in plant leaves with reflectance spectroscopy. *Photochem. Photobiol.* **2002**, *75*, 272–281. [CrossRef]

42. Gamon, J.A.; Peñuelas, J.; Field, C.B. A narrow-waveband spectral index that tracks diurnal changes in photosynthetic efficiency. *Remote Sens. Environ.* **1992**, *41*, 35–44. [CrossRef]

43. Gamon, J.A.; Huemmrich, K.F.; Wong, C.Y.S.; Ensminger, I.; Garrity, S.; Hollinger, D.Y.; Noormets, A.; Peñuelas, J. A remotely sensed pigment index reveals photosynthetic phenology in evergreen conifers. *Proc. Natl. Acad. Sci. USA* **2016**, *113*, 13087–13092. [CrossRef]

44. Costa, J.M.; Grant, O.M.; Chaves, M.M. Thermography to explore plant-environment interactions. *J. Exp. Bot.* **2013**, *64*, 3937–3949. [CrossRef]

45. Kefauver, S.C.; Vicente, R.; Vergara-Díaz, O.; Fernandez-Gallego, J.A.; Kerfal, S.; Lopez, A.; Melichar, J.P.E.; Serret Molins, M.D.; Araus, J.L. Comparative UAV and Field Phenotyping to Assess Yield and Nitrogen Use Efficiency in Hybrid and Conventional Barley. *Front. Plant Sci.* **2017**, *8*, 1–15. [CrossRef]

46. Cerovic, Z.G.; Masdoumier, G.; Ghozlen, N.B.; Latouche, G. A new optical leaf-clip meter for simultaneous non-destructive assessment of leaf chlorophyll and epidermal flavonoids. *Physiol. Plant.* **2012**, *146*, 251–260. [CrossRef]

47. Cerovic, Z.G.; Ghozlen, N.B.; Milhade, C.; Obert, M.; Debuisson, S.; Le Moigne, M. Nondestructive Diagnostic Test for Nitrogen Nutrition of Grapevine (*Vitis vinifera* L.) Based on Dualex Leaf-Clip Measurements in the Field. *J. Agric. Food Chem.* **2015**, *63*, 3669–3680. [CrossRef]

48. RStudio Team. *RStudio: Integrated Development for R*; RStudio, Inc.: Boston, MA, USA; Available online: http://www.rstudio.com/ (accessed on 12 September 2018).

49. *R Core Team R: A Language and Environment for Statistical Computing*; R Foundation for Statistical Computing: Vienna, Austria, 2017.

50. Alvarado, G.; López, M.; Vargas, M.; Pacheco, Á.; Rodríguez, F.; Burgueño, J.; Crossa, J. META-R (Multi Environment Trail Analysis with R for Windows) Version 6.01. 2017. Available online: https://data.cimmyt.org/dataset.xhtml?persistentId=hdl:11529/10201/ (accessed on 16 December 2018).

51. Prasad, P.V.V.; Staggenborg, S. Impacts of drought and/or heat stress on physiological, developmental, growth, and yield processes of crop plants. In *Response of Crops to Limited Water: Understanding and Modeling Water Stress Effects on Plant Growth Processes Response of Crops*; American Society of Agronomy: Madison, WI, USA, 2008; pp. 301–355.

52. Farooq, M.; Bramley, H.; Palta, J.A.; Siddique, K.H.M. Heat Stress in Wheat during Reproductive and Grain-Filling Phases. *Crit. Rev. Plant Sci.* **2011**, *30*, 491–507. [CrossRef]

53. Pinto, R.S.; Molero, G.; Reynolds, M.P. Identification of heat tolerant wheat lines showing genetic variation in leaf respiration and other physiological traits. *Euphytica* **2017**, *213*, 1–15. [CrossRef]

54. Rashid, M.A.; Andersen, M.N.; Wollenweber, B.; Kørup, K.; Zhang, X.; Olesen, J.E. Impact of heat-wave at high and low VPD on photosynthetic components of wheat and their recovery. *Environ. Exp. Bot.* **2018**, *147*, 138–146. [CrossRef]

55. Long, S.P.; Ort, D.R. More than taking the heat: Crops and global change. *Curr. Opin. Plant Biol.* **2010**, *13*, 241–248. [CrossRef]

56. Torriani, D.S.; Calanca, P.; Schmid, S.; Beniston, M.; Fuhrer, J. Potential effects of changes in mean climate and climate variability on the yield of winter and spring crops in Switzerland. *Clim. Chang.* **2007**, *34*, 59–69. [CrossRef]

57. Ghahramani, A.; Kokic, P.N.; Moore, A.D.; Zheng, B.; Chapman, S.C.; Howden, M.S.; Crimp, S.J. The Value of Adapting to Climate Change in Australian Wheat Farm Systems: Farm to Cross-Regional Scale. *Agric. Ecosyst. Environ.* **2015**, *211*, 112–125.

58. Nouri, M.; Homaee, M.; Bannayan, M.; Hoogenboom, G. Towards shifting planting date as an adaptation practice for rainfed wheat response to climate change. *Agric. Water Manag.* **2017**, *186*, 108–119. [CrossRef]

59. Weiss, A.; Hays, C.J.; Won, J. Assessing winter wheat responses to climate change scenarios: A simulation study in the U.S. *Great Plains.* **2003**, *58*, 119–147.

60. Altenbach, S.B.; DuPont, F.M.; Kothari, K.M.; Chan, R.; Johnson, E.L.; Lieu, D. Temperature, water and fertilizer influence the timing of key events during grain development in a US spring wheat. *J. Cereal Sci.* **2003**, *37*, 9–20. [CrossRef]

61. Fernandez-gallego, J.A.; Kefauver, S.C.; Vatter, T. Low-cost assessment of grain yield in durum wheat using RGB images. *Eur. J. Agron.* **2019**, *105*, 146–156. [CrossRef]

62. Snape, J.W.; Butterworth, K.; Whitechurch, E.; Worland, A.J. Waiting for fine times: Genetics of flowering time in wheat. *Euphytica* **2001**, *119*, 185–190. [CrossRef]

63. Asana, R.D.; Mani, V.S. Studies in Physiological Analysis of Yield. II. Further Observations on Varietal Differences in Photosynthesis in the Leaf, Stem and Ear of Wheat. *Physiol. Plant.* **1955**, *8*, 8–19. [CrossRef]

64. Ugarte, C.; Calderini, D.F.; Slafer, G.A. Grain weight and grain number responsiveness to pre-anthesis temperature in wheat, barley and triticale. *Field Crops Res.* **2007**, *100*, 240–248. [CrossRef]

65. González, F.G.; Slafer, G.A.; Miralles, D.J. Grain and floret number in response to photoperiod during stem elongation in fully and slightly vernalized wheats. *Field Crops Res.* **2003**, *81*, 17–27. [CrossRef]

66. Lukina, E.V.; Stone, M.L.; Raun, W.R. Estimating vegetation coverage in wheat using digital images. *J. Plant Nut.* **1999**, *22*, 341–350. [CrossRef]

67. Cabrera-Bosquet, L.; Molero, G.; Stellacci, A.M.; Bort, J.; Nogues, S.; Araus, J.L. NDVI as a potential tool for predicting biomass, plant nitrogen content and growth in wheat genotypes subjected to different water and nitrogen conditions. *Cereal Res. Commun.* **2011**, *39*, 147–159. [CrossRef]

68. Duan, T.; Chapman, S.C.; Guo, Y.; Zheng, B. Field Crops Research Dynamic monitoring of NDVI in wheat agronomy and breeding trials using an unmanned aerial vehicle. *Field Crops Res.* **2017**, *210*, 71–80. [CrossRef]

69. Gregersen, P.L.; Culetic, A.; Boschian, L.; Krupinska, K. Plant senescence and crop productivity. *Plant Mol. Biol.* **2013**, *82*, 603–622. [CrossRef] [PubMed]

70. Thomas, H.; Ougham, H. The stay-green trait. *J. Exp. Bot.* **2014**, *65*, 3889–3900. [CrossRef]

71. Christopher, J.; Veyradier, M.; Borrell, A.; Harvey, G.; Fletcher, S.; Chenu, K. Phenotyping novel stay-green traits to capture genetic variation in senescence dynamics. *Funct. Plant Biol.* **2014**, *41*, 1035–1048. [CrossRef]

72. Christopher, J.T.; Christopher, M.J.; Borrell, A.K.; Fletcher, S.; Chenu, K. Stay-green traits to improve wheat adaptation in well- watered and water-limited environments. *J. Exp. Bot.* **2016**, *67*, 5159–5172. [CrossRef]

73. Spano, G.; Di Fonzo, N.; Perrotta, C.; Platani, C.; Ronga, G.; Lawlor, D.W.; Napier, J.A. Physiological characterization of stay green mutants in durum wheat. *J. Exp. Bot.* **2003**, *54*, 1415–1420. [CrossRef] [PubMed]

74. Crain, J.; Reynolds, M.; Poland, J. Utilizing High-Throughput Phenotypic Data for Improved Phenotypic Selection of Stress-Adaptive Traits in Wheat. *Crop Sci.* **2017**, *659*, 648–659. [CrossRef]

75. Lopes, M.S.; Reynolds, M.P. Stay-green In Posidonia in oceanica spring wheat cadmium can be induces determined changes by in spectral DNA reflectance methylation measurements and chromatin (normalized patterning difference vegetation index) independently from phenology. *J. Exp. Bot.* **2012**, *63*, 3789–3798. [CrossRef] [PubMed]

76. Kichey, T.; Hirel, B.; Heumez, E. In winter wheat (*Triticum aestivum* L.), post-anthesis nitrogen uptake and remobilisation to the grain correlates with agronomic traits and nitrogen physiological markers. *Field Crop Res.* **2007**, *102*, 22–32. [CrossRef]

77. Derkx, A.P.; Orford, S.; Griffiths, S.; Foulkes, M.J.; Hawkesford, M.J. Identification of Differentially Senescing Mutants of Wheat and Impacts on Yield, Biomass and Nitrogen. *J. Integr. Plant Biol.* **2012**, *54*, 555–566. [CrossRef]

78. Buchaillot, M.L.; Gracia-Romero, A.; Vergara-Diaz, O.; Zaman-Allah, M.A.; Tarekegne, A.; Cairns, J.E.; Prasanna, B.M.; Araus, J.L.; Kefauver, S.C. Evaluating Maize Genotype Performance under Low Nitrogen Conditions Using RGB UAV Phenotyping Techniques. *Sensor* **2019**, *19*, 1815. [CrossRef] [PubMed]

79. Monostori, I.; Árendás, T.; Hoffman, B.; Galiba, G.; Gierczik, K.; Szira, F.; Vágújfalvi, A. Relationship between SPAD value and grain yield can be affected by cultivar, environment and soil nitrogen content in wheat. *Euphytica* **2016**, *211*, 103–112. [CrossRef]

80. Gamon, J.A.; Serrano, L.; Surfus, J.S. The photochemical reflectance index: An optical indicator of photosynthetic radiation use efficiency across species, functional types, and nutrient levels. *Oecologia* **1997**, *112*, 492. [CrossRef] [PubMed]

81. Peñuelas, J.; Garbulsky, M.F.; Filella, I. Photochemical reflectance index (PRI) and remote sensing of plant CO_2 uptake. *New Phytol.* **2011**, *191*, 596–599. [CrossRef] [PubMed]

82. Magney, T.S.; Vierling, L.A.; Eitel, J.U.H.; Huggins, D.R.; Garrity, S.R. Response of high frequency Photochemical Reflectance Index (PRI) measurements to environmental conditions in wheat. *Remote Sens. Environ.* **2016**, *173*, 84–97. [CrossRef]

83. Loss, S.P.; Siddique, K.H.M. *Morphological and Physiological Traits Associated with Wheat Yield Increases in Mediterranean Environments*; Sparks, D.L., Ed.; Academic Press: Boston, MA, USA, 1994; Volume 52, pp. 229–276.

84. Villegas, D.; Aparicio, N.; Royo, C. Assessment of durum wheat yield and carbon isotope discrimination by reflectance indices WI and PRI. In *Cereal Science and Technology for Feeding Ten Billion People: Genomics Era and beyond*; Options Méditerranéennes: Série A. Séminaires Méditerranéens: Zaragoza, Spain, 2008; Volume 81, pp. 403–405.

85. Araus, J.L.; Bort, J.; Steduto, P.; Villegas, D.; Royo, C. Breeding cereals for Mediterranean conditions: Ecophysiological clues for biotechnology application. *Ann. Appl. Biol.* **2003**, *142*, 129–141. [CrossRef]

86. Fischer, R.A.; Rees, D.; Sayre, K.D.; Lu, Z.-M.; Condon, A.G.; Saavedra, A.L. Wheat Yield Progress Associated with Higher Stomatal Conductance and Photosynthetic Rate, and Cooler Canopies. *Crop Sci.* **1998**, *38*, 1467–1475. [CrossRef]

87. Berger, B.; Parent, B.; Tester, M. High-throughput shoot imaging to study drought responses. *J. Exp. Bot.* **2010**, *61*, 3519–3528. [CrossRef]

88. Aparicio, N.; Villegas, D.; Casadesus, J.; Araus, J.L.; Royo, C. Spectral vegetation indices as nondestructive tools for determining durum wheat yield. *Agron. J.* **2000**, *92*, 83–91. [CrossRef]

89. Crain, J.; Mondal, S.; Rutkoski, J.; Singh, R.P.; Poland, J. Combining High-Throughput Phenotyping and Genomic Information to Increase Prediction and Selection Accuracy in Wheat Breeding. *Plant Genome* **2018**, *11*, 1–14. [CrossRef]

90. Petersen, L.K. Real-Time Prediction of Crop Yields From MODIS Relative Vegetation Health: A Continent-Wide Analysis of Africa. *Remote Sens.* **2018**, *10*, 1726. [CrossRef]

91. Torres-Sánchez, J.; Peña, J.M.; Castro, A.I. Multi-temporal mapping of the vegetation fraction in early-season wheat fields using images from UAV. *Comput. Electron. Agric.* **2014**, *103*, 104–113. [CrossRef]

92. Stöcker, C.; Bennett, R.; Nex, F.; Gerke, M.; Zevenbergen, J. Review of the current state of UAV regulations. *Remote Sens.* **2017**, *9*, 459. [CrossRef]

93. Gago, J.; Douthe, C.; Coopman, R.E.; Gallego, P.P.; Ribas-Carbo, M.; Flexas, J.; Escalona, J.; Medrano, H. UAVs challenge to assess water stress for sustainable agriculture. *Agric. Water Manag.* **2015**, *153*, 9–19. [CrossRef]

94. Sudhakar, P.; Latha, P.; Reddy, P.V. *Phenotyping Crop Plants for Physiological and Biochemical Traits*; Academic Press: Boston, MA, USA, 2016.

95. Piepho, H.P.; Möhring, J. Computing heritability and selection response from unbalanced plant breeding trials. *Genetics* **2007**, *177*, 1881–1888. [CrossRef]